Vol. 10(4), pp. 85-100, July-December 2019
DOI: 10.5897/JPGE2019.0311
Article Number: C6F9A2661863
ISSN: 2141-2677

http://www.academicjournals.org/JPGE

ACADEMIC JOURNALS
expand your knowledge

Journal of Petroleum and Gas Engineering

Full Length Research Paper

Evaluating the performance of ultrasound energy on improved oil recovery using MATLAB reservoir simulation toolbox (MRST)

Usman Hassan[1*], Joseph Atubokiki Ajienka[1] and Alhaji Dodo Ibrahim Sulaiman[2]

[1]Department of Petroleum Engineering, World Bank Africa, Centre for Oilfield Chemicals Research, University of Port Harcourt, Nigeria.
[2]Department of Petroleum Engineering, Faculty of Engineering, Abubakar Tafawa Balewa University Bauchi, Nigeria.

Received 26 February, 2019; Accepted 26 March, 2019

There are many processes the oil industry used to recover more oil from the reservoir after the natural energy is depleted. In this research work, ultrasound energy has been tested as a method of improving oil recovery after waterflooding. The method used in this research work was a numerical simulation using MATLAB Reservoir Simulation Toolbox (MRST-2017a). Ultrasound energy source equation was incorporated into the residual energy equation in the MRST. Acoustic attenuation pressure equation was modelled as part of the residual pressure equation in the MRST. Effect of ultrasound waves on pore wall deformation was also modelled from waves stress equation. Two-phase (oil/water) black oil model was used to simulate fluid flow. Results obtained from the simulation runs show that the ultrasound energy has an impact on reservoir performance i.e. increase in fluid flowrates and pore pressure and temperature rise which led to oil viscosity reduction and consequently improve mobility ratio. However, attenuation of ultrasound energy increases with propagation distance, but this effect was compensated by increasing the intensity of the ultrasound power. Though, high power intensity induced stress on the reservoir pore throat. Results obtained also show that high porosity and permeability values affect the performance of the acoustic energy basically due to an increase in the rate of waves absorption.

Key words: Ultrasound energy, improved oil recovery, reservoir simulation toolbox, MATLAB.

INTRODUCTION

Recovering a substantial part of oil reserve has become a great challenge to the oil industry. There are many research works on improving the recovery factor of reservoir oil. Most methods of improving oil recovery factor presently used by industries are associated with some challenges and limitations. However, many researchers have been making efforts to address those challenges and limitations.

The quest by researchers to develop more effective, efficient and economical ways of improving oil recovery has led to the invention and innovation of various techniques of enhancing reservoir oil production. After the natural energy locked up in the reservoir (*in-situ* energy) is depleted, the common practice by E&P operators to augment the primary energy is pressure maintenance, which is basically water injection or gas injection. General practice is; water is injected through injection well(s) to the production zone or gas is injected

*Corresponding author. E-mail: shingasco@gmail.com.

to the gas cap to push the oil towards production well.

The limit of the secondary recovery is reached when the volume of the injected fluid (water or gas) become excess in the produced fluid, thereby overloading the production facilities and making oil production uneconomical. Many pieces of research have been carried out on how to increase oil recovery after the secondary recovery is no longer economical. Those methods employed to improve oil recovery after the secondary recovery is referred to as enhanced oil recovery methods or tertiary oil recovery methods. Generally, accepted enhanced oil recovery methods by exploration and production companies are chemical flooding, thermal method and miscible gas method. The choice for each of the methods depends on the: reservoir rock characteristics, reservoir fluid properties and economic consideration. Each of the above-mentioned enhanced oil recovery methods has some challenges and limitations which led to the invention of many recovery methods that can mitigate those challenges. The following are some new approaches to enhance oil recovery:

(i) Microbial enhanced oil recovery
(ii) Nanoparticles enhanced oil recovery
(iii) High-frequency waves
(iv) *In-situ* reservoir electric heating
(v) Vapour extraction VAPEX etc.

There are research works on the application of ultrasound energy to enhance oil recovery. These works include; laboratory experiments, field test and very few software simulations.

Laboratory experiment

Erfan et al. (2011) conducted an experiment to check the effect of ultrasonic waves in enhancing oil recovery during waterflooding. During the experiment, kerosene and vaseline were used as the non-wetting phases in the experiment. And an unconsolidated sand pack was used as the porous media. At the end of the experiment, 16% oil recovery increment was observed. The mechanisms that caused the increment in oil recovery were identified as viscosity reduction and emulsification.

An ultrasonic stimulation and waterflooding experiment were conducted by Mohammadian et al. (2013) on an unconsolidated sand pack, where the non-wetting phase used in the system were; engine oil, kerosene, and vaseline. In this, up to 16% oil recovery was observed. The mechanisms that contributed to the increase in recovery were identified as; cavitation and emulsification. Alhomadhi et al. (2014) carried out a laboratory experiment on reservoir rock core samples to investigate the ability of ultrasound waves to improve oil production (Figure 1). The ultrasound wave was applied to the core samples after performing initial waterflooding. The experiment was conducted at original oil in place and at residual oil saturation. The results of this work show that; oil recovery factor is more favourable in the case of residual oil saturation than the case of original oil in place.

An experiment was carried out by Delong et al. (2014) on the application of ultrasonic wave to reduce the viscosity of ultra heavy crude oil in water. Fengcheng and Venezuela ultra heavy crude oil (UHCO) were used in the experiment, and the viscosity reduction resulting from the ultrasound wave effect was found to be more than 25%. Mohammed and Mahmoud (2015) developed a model for using ultrasonic waves to enhance oil recovery in oil field reservoirs. The model is modular and comprises an acoustic and heat transfer modules (Figure 2). The model considers both the geophysical and acoustic properties of a well. Ultrasonic waves of 20 kHz frequency and output power of 350 W were used in the experiment. About 82% oil recovery was observed from the experiment.

Field test

Abramova et al. (2014) designed and developed downhole equipment for ultrasonic oil production enhancement. The equipment includes a sonotrode PSMS-42 and a geophysical data (temperature, pressure and flow) registrator. Field tests were carried out using the developed ultrasonic downhole tool PSMS-42. The results obtained from the tests show a good efficiency of the proposed technology. About 90% of this method was achieved and 40 - 100% oil recovery was observed (Figure 3).

According to Mullakaev et al. (2015), after ultrasound stimulation was conducted on three wells, an average increase of 32.6 barrels of oil per day was observed, and the effect of the treatment on oil production was about six months. During the treatment, fluid was injected to aid wave propagation (Figure 4) for equipment arrangement at the wellhead.

Field tests on ultrasonic treatment were conducted at Samara Region (SR) and Western Siberia (WS). According to Mullakaev et al. (2015), more than 100 operations were carried out for the period between 2010 to 2012, and the average production rate increase that was observed after the start of the operation was 10.2 tons for Samara Region and 4.4 tons for Western Siberia. Several field tests have also been carried out with the application of ultrasonic waves to oil fields for improved oil recovery and the results were positive in Texas, Siberia and California (Naderi and Babadagli, 2010).

Software simulation

Software simulation was also carried out by Mohammed

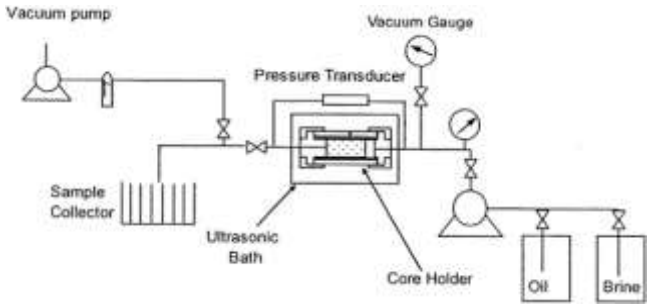

Figure 1. Experimental set up used by Alhomadhi el al. (2014).

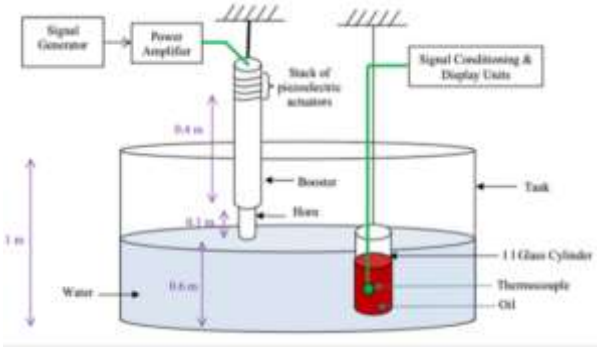

Figure 2. Experimental set up used by Mohammed and Mahmoud (2015).

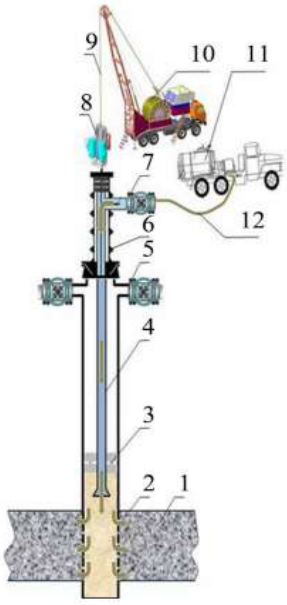

Figure 3. Hardware elements arrangement during ultrasonic treatment: 1) oil reservoir, 2) ultrasonic downhole equipment 3) packer 4) tubing 5) casing valve 6) lubricator 7) flowout line 8) cable feed 9) cable 10) wire line II KC-5 11) pump unit CNH-32 12) hose (Abramova et al., 2014).

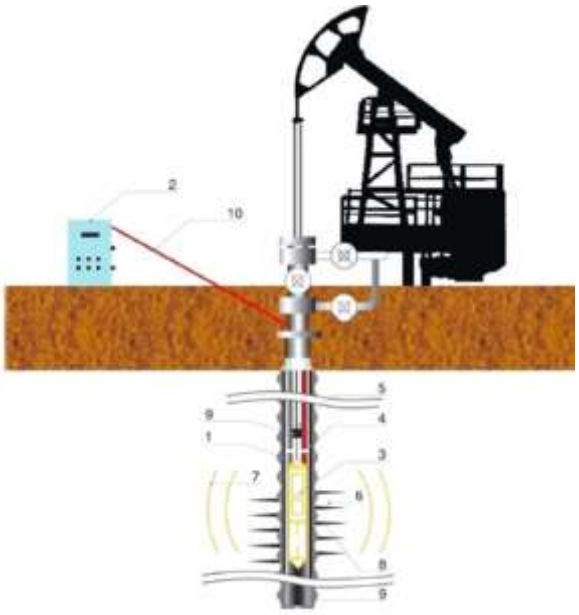

Figure 4. Equipment configuration for near-well treatment using PSMS-102 1) Anchor 2) Ultrasonic generator 3) Downhole 4) Casing 5) Tubing 6) Producing formation 7) Ultrasonic field 8) Perforated zone 9) Sucker rod pump 10) Downhole tool power cable (Mullakaev et al., 2015).

and Mahmoud (2015) for comparison between experimental results and that of the software and to validate the results of their experiment.

The numerical simulation was performed using finite element-based method. Darcy flow model coupled with acoustic pressure in COMSOL multiphysics has been used to evaluate the pressure and temperature distribution in the target medium when exposed to ultrasound waves. Figures 5 and 6 show the pressure and temperature distribution respectively.

A lead-in to the simulation toolbox (MRST)

Software modelling and simulation provide a solution to real life problems easily and efficiently; software simulation is more flexible and faster than real life or practical experiment; moreover, it is cheaper and safer. However, it is imperative to validate simulation results with a practical experiment or field test which appeared to be more natural.

MATLAB reservoir simulation toolbox (MRST) is an open source reservoir simulator developed by SINTEF Applied Mathematics as a MATLAB toolbox, but it is not primarily a simulator. MRST consists of two sections: a core offering basic functionality and some single and two-phase solvers, along with a set of add-on modules offering more advanced models, viewers and solvers (Knut-Andreas, 2016). MRST provides large sets of data structures and a wide range of computational methods

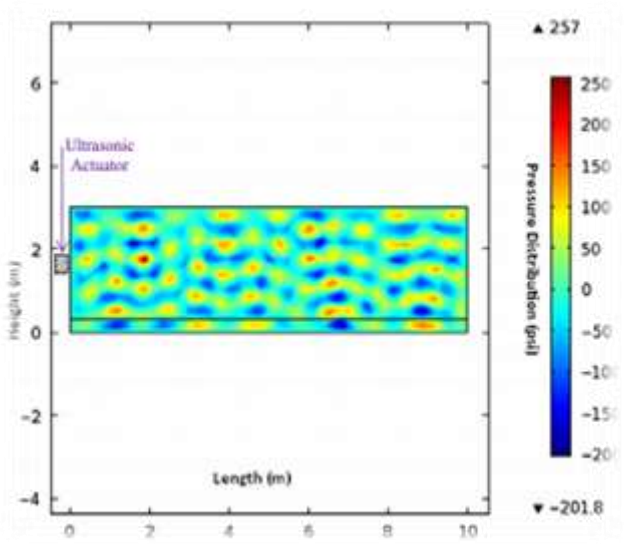

Figure 5. Pressure distribution in oil reservoir model Mohammed and Mahmoud (2015).

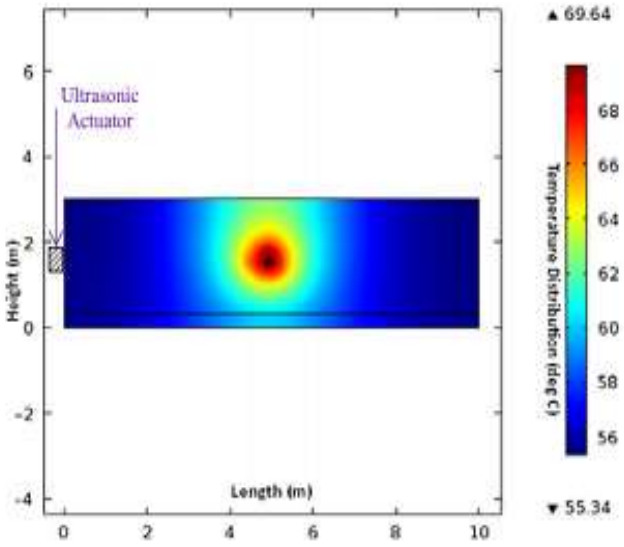

Figure 6. Temperature distribution in oil reservoir model Mohammed and Mahmoud (2015).

that can easily be used to develop customized modelling and simulation tools.

Availability of commercial or open source software that can be used to simulate the application of ultrasound energy to improve oil recovery is challenging. This research paper is aimed at modelling a reservoir and simulating the effect of applying ultrasound energy on reservoir performance using MRST. Black-oil, two-phase (oil-water) system and ultrasound energy were modelled and simulated using the MRST package.

METHODOLOGY

The approach to this work is the development of numerical simulator using MATLAB Reservoir Simulator Toolbox (MRST). The MRST was modified to suit the objectives of the work. The following are the step by step procedure that was followed to build the simulator (Figure 7).

Geological model and grid

In order to model the heterogeneity of the reservoir, a geostatistical method was used to make realizations of porosity and permeability. The porosity (ϕ) data were generated using Gaussian field distribution as shown in Figure 8. The permeability (k) data were generated using Carman-Kozeny relation (Dvorkin, 2009).

$$k = \frac{1}{8\tau A_v^2}\frac{\phi^3}{(1-\phi)^2} \quad (1)$$

Where: A_v is the specific surface area, that is, (the internal surface area per unit volume of any porous media) and τ is the tortuosity. Figure 9 shows the permeability distribution.

Cartesian grid blocks in 3D cubic domain was used for easy discretization of flow equations.

Well models

Single production well was modelled and vertically positioned at the centre of the grid block (reservoir) as shown in Figure 9.

Compressibility model

Rock compressibility (c_r) describes the relationship between the porosity and pressure (p) as shown in Equation 2.

$$c_r = \frac{d\ ln(\phi)}{d_p} \quad (2)$$

And the fluid compressibility relates the density (ρ) and pressure of the fluid as shown in Equation 3.

$$c_f = \frac{1}{\rho}\frac{d\rho}{dp} = \frac{d\ \ln(\rho)}{dp} \quad (3)$$

The total compressibility (c_t) = c_r + c_f

Flow equations model

Fluid fluxes through the control volume and through the boundary surfaces (S) where some quantity can be conserved in the volume O (Figure 10). The conservation of mass equation is given in the integral form as shown in Equation 4 (Knut-Andreas, 2016):

$$\int_O \frac{\partial u}{\partial t}dv + \int_S \vec{F}.\vec{n}\,ds = \int_O Q dv \quad (4)$$

The first integral sums up the change in mass per second in the volume O, the second integral accounts for boundary flow and interlocks mass transfer through the boundary, and the right-hand side accounts for fluid source or sink. Using the Gauss divergence

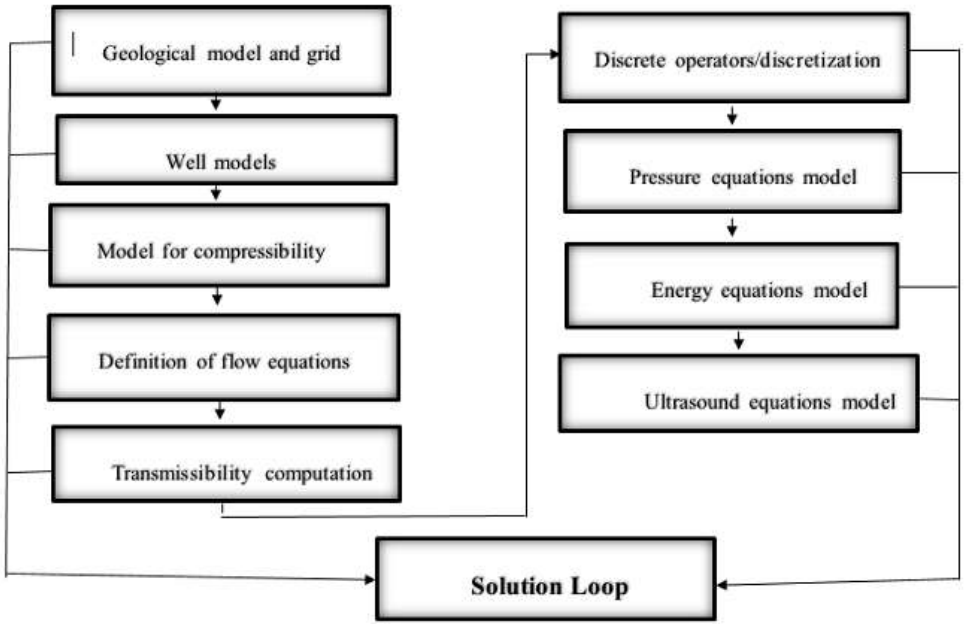

Figure 7. Modelling flowchart.

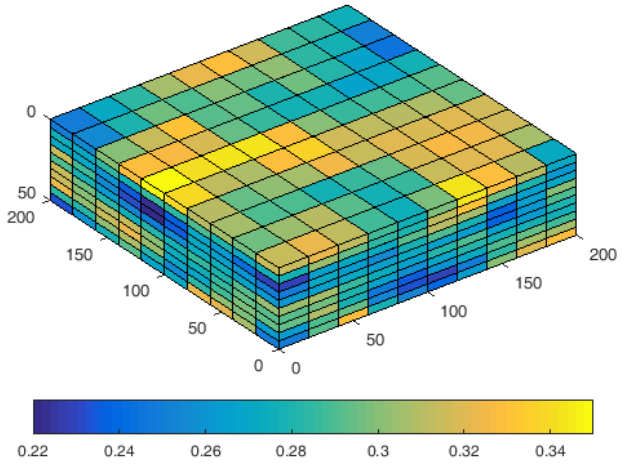

Figure 8. Gaussian field porosity distribution.

theorem and substituting flux and velocity terms in Equation 4, the general conservation of mass is given by Equation 5.

$$\frac{\partial(\rho\phi S)}{\partial t} + \nabla.(\rho\lambda(\nabla p + \gamma\nabla h) = Q \quad (5)$$

where: ρ = density of fluid phase, ϕ = rock porosity, S = fluid saturation, λ = phase mobility, ∇p = pressure gradient, γ = specific gravity, ∇h = vertical depth.

Black oil two phase (oil-water) model

For two phase oil-water system, the conservation equation in 5 was used to model the general pressure equation after substituting the wetting (*W*) and non-wetting (*O*) phases pressure and saturation equations is given by Equation 6.

$$\phi c_T \frac{\partial \rho_w}{\partial t} + \phi S_o c_o \frac{\partial p_c}{\partial t} + \frac{1}{\rho_w}.\nabla(\rho_w \vec{v}_w) + \frac{1}{\rho_o}.\nabla(\rho_o \vec{v}_o) = \frac{q_w}{\rho_w} + \frac{q_o}{\rho_o} \quad (6)$$

where: $c_T = S_w c_w + S_o c_o$ assuming zero change in porosity with time.

Solution strategy

For the scope of this work, finite volume method was used to discretize the accumulation terms (A&B) in equation 6 temporal in

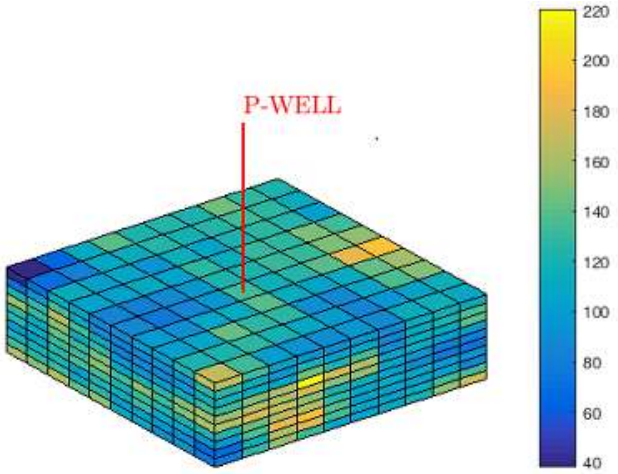

Figure 9. Permeability distribution.

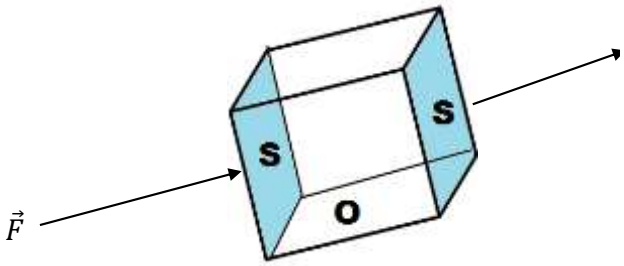

Figure 10. Schematic representation of a control volume with boundary surface S and volume O.

time and the flux terms were approximated using two-point flux approximation scheme (TPFA). The coupled scheme can be solved for p_w explicitly.

$$A = \phi c_T \left(\frac{p_{wi}^{n+1} - p_{wi}^{n}}{\Delta t}\right) \tag{7}$$

$$B = \phi S_o c_o \left(\frac{p_c(t+\Delta t) - p_c(t)}{\Delta t}\right) \tag{8}$$

Where p_c in Equation 8 can be obtained from the Van Ganuchten capillary pressure (Christine, 2013) shown in Equation 9.

$$p_c(t) = \left[\frac{\frac{1}{(S_{e1})^z} - 1}{\propto}\right]^{\frac{1}{n}} \tag{9}$$

Using tailor's series, equation 9 can be written as;

$$p_c(t+\Delta t) = \left[\frac{\frac{1}{(S_{e2})^z} - 1}{\propto}\right]^{\frac{1}{n}} \tag{10}$$

Where:

$$z = \frac{n}{n-1} \tag{11}$$

$$S_e = \frac{S - S_r}{1 - S_r} \tag{12}$$

S_e is the effective saturation, S_r residual saturation and n Van Ganuchten parameter.
At each time step, the capillary pressure has a single value averaged across the entire reservoir.

Two-point flux approximation scheme

For advective/horizontal flow, we assume two active flux boundaries between cells in the global grid as shown in Figure 11. Flux is given by the vector integral in Equation 13.

$$V_{i,k} = \int_{S_{ik}} \vec{u} \,.\, \vec{n}\, ds \tag{13}$$

$$V_{i,k} \approx A_{i,k}\vec{V}\left(\vec{x}_{i,k}\right).\vec{n}_{i,k} = -A_{i,k}(k\nabla p)\left(\vec{x}_{i,k}\right).\vec{n}_{i,k} \tag{14}$$

After substitutions and expansions, the flux approximations for oil and water for the flux terms in Equation 6 are shown in Equations 15 and 16:

Oil:

$$\vec{F}_O = \frac{\rho_o T_{i,k}\,(p_i - p_k)}{\mu_o} \tag{15}$$

Water:

$$\vec{F}_w = \frac{\rho_w T_{i,k}\,(p_i - p_k)}{\mu_w} \tag{16}$$

Substituting Equations 7, 8, 15 and 16 in Equation 6 give Equation 17.

$$\phi c_T\left(\frac{p_{wi}^{n+1} - p_{wi}^{n}}{\Delta t}\right) + \phi S_o c_o\left(\frac{p_c(t+\Delta t) - p_c(t)}{\Delta t}\right) + \frac{1}{\rho_w}\left(\frac{\rho_w T_{i,k}\,(p_i - p_k)}{\mu_w}\right) + \frac{1}{\rho_o}\frac{\rho_o T_{i,k}\,(p_i - p_k)}{\mu_o} = Q \tag{17}$$

Making p_{wi}^{n+1} subject of formula, Equation 17 changed to 18 which is the general water pressure solution for the two phase (oil-water) black oil model.

$$p_{wi}^{n+1} = p_{wi}^{n} + \frac{\Delta t}{\phi C_T}\left[Q - \phi S_o C_o\left(\frac{\Delta p_c}{\Delta t}\right) - \frac{T_{i,k}(p_i - p_k)}{\mu_w} - \frac{T_{i,k}(p_i - p_k)}{\mu_o}\right] \tag{18}$$

After finding the values of water pressure (p_w) at different time levels, the initial oil pressure can be computed from Equation 19:

$$p_c = p_{oil} - p_w \tag{19}$$

Energy equations model

Assuming only a single-phase oil energy equation that is, the oil and rock neglecting connate water saturation heat. Due to the

above fact it is also assume that $\rho(p,T)$, density a function of temperature and pressure, then the energy conservation equation becomes:

$$\frac{\partial}{\partial t}[\phi\rho] + \nabla.[\rho\vec{v}] = q \tag{20}$$

Where: $\vec{v} = \frac{-k}{\mu}[\nabla p - g\rho\nabla z]$ darcy velocity

The general energy conservation is given by Equation 21.

$$\underbrace{\frac{\partial}{\partial t}\left[\phi\rho E_f(p,T) + (1-\phi)E_r\right]}_{\text{Energy accumulation}} + \underbrace{\nabla.\left[\rho H_f\vec{v}\right]}_{\text{Heat flux at the boundaries}} - \underbrace{\nabla.[K\nabla T]}_{\text{Conductive heat loss}} = \underbrace{q_e}_{\text{Ultrasound source}} \tag{21}$$

Where: ϕ = porosity, ρ = density, E_f = fluid energy density, E_r = rock energy density, H_f = enthalphy, K = heat conduction co-efficient.

$$H_f = E_f + \frac{p}{\rho} \tag{22}$$

$$dH_f = C_p dT + \left(\frac{1-\propto T_r}{\rho}\right)dp \tag{23}$$

The constitutive relationships for pressure and temperature dependent density and viscosity are shown in Equations 24 and 25 respectively:

$$\rho(P,T) = \rho_r[1 + \beta_T(p - p_r)]e^{-\propto(T-T_r)} \tag{24}$$

$$\mu(P,T) = \mu_o\left[1 + C_\mu(p - p_r)\right]e^{-C_T(T-T_r)} \tag{25}$$

The following equations (26 and 27) are the residual pressure and energy equations for oil in MRST

$$p_{eq} = \frac{1}{\Delta t}\left[pv.\rho\left(P,T\right) - pv(p_o)\rho\left(P_o,T_o\right)\right] + div[\rho * \vec{v}] \tag{26}$$

$$h_{Eq} = \frac{1}{\Delta t}\left[pv.\rho.E_f + sv.E_r\right] + div\left[\rho H_f\vec{v}\right] - div[Th.gradT] \tag{27}$$

Ultrasonic output power

The average output power generated by ultrasound is given by Equation 28 (Aarts et al., 1999):

$$W = \frac{L^2|p-p_o|^2(2\pi f)}{\rho\mu} \tag{28}$$

Where: W = average transducer output power, f = ultrasound frequency, L = distance between transducer and the porous media, ρ, μ = density and viscosity of the medium, $|p - p_o|$ = amplitude of acoustic excess pressure.

The ultrasound power equation (Equation 28) was used to know how the reservoir fluid properties, waves frequency and the location of the sound source affects the power intensity of the ultrasound waves. However, the ultrasound powers used in the simulation runs were selected arbitrarily to represent the power that will be generated from the ultrasound generating system.

Pore wall deformation from ultrasound energy

It is assumed that the pore walls will be deformed due to stress exerted on the walls by ultrasonic energy irradiation. Figure 12 shows the pore wall deformation. The stress created by ultrasound energy is given by Equation 28.

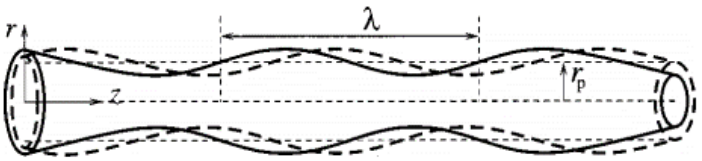

Figure 12. Pore wall deformation caused by ultrasound energy (Aarts et al., 1999).

$$\sigma_f = \sigma_i * \sin(\omega t + q) \tag{28}$$

Where: σ_f, σ_i = final and initial stresses
ω = angular frequency $(2\pi f)$
q = phase shift

$$\sigma = \frac{force}{area} \tag{29}$$

$$area = \pi(r_p + a) \tag{30}$$

The reservoir rock is assumed to be slightly elastic, therefore the corresponding strain is given in Equation 31.

$$\varepsilon_f = \varepsilon_i * \sin(\omega t) \tag{31}$$

$$strain = \frac{stress}{bulk\ \ modulus} \tag{32}$$

Attenuation of ultrasound energy

The attenuation of acoustic pressure as a function of propagation distance is shown in Equation 33 (Chen and Holm, 2003).

$$p(x + \Delta x) = p(x)e^{-\alpha\omega\Delta x} \tag{33}$$

Where: p = acoustic pressure
Δx = propagation distance
α, ω = attenuation coefficient, angular frequency

Simulation process

The set of data used for the simulation process are presented in Table 1.

RESULTS

The simulation was initially carried out without ultrasound energy, Figure 13 shows how the reservoir oil flow rate declines with time when no external energy was applied to the reservoir. Decline in pressure regime (minimum, average and maximum) with time is shown in Figure 14. Both the pressures and flowrate continue to decline with time from the initial values to zero when no ultrasound

Table 1. Data set used in the simulation runs.

Description	Quantity/symbol	Value/unit		
Average Rock Properties	Grid block D_x x D_y x D_z	i.	200 x 200 x 50 ft	
		ii.	400 x 400 x 50 ft	
	Porosity distribution		Max	Min %
	ϕ	i.	0.35	0.22
		ii.	0.31	0.21
		iii.	0.30	0.20
			Min	Max md
	Permeability distribution $k_x = k_y = k_z$	i.	40	220
		ii.	30	130
		iii.	20	110
	Rock compressibility c_r	$1x10^{-6}$ /bar		
	Average pressure p_r	200 bar		
	Average temperature T_r	300 kelvin		
Fluid properties				
	Oil density ρ_w	870 kg/m^3		
	Water density ρ_w	1014 kg/m^3		
	Oil viscosity μ_o	5.0 cp		
Ultrasound properties	Water viscosity μ_o	1.0 cp		
	Water compressibility c_w	$2x10^{-6}$/psia		
	Oil compressibility c_o	$1x10^{-5}$/psia		
	Output power P	5 kW, 6 kW, 7 kW		
	Frequency f	20 kHz		
	Propagation distance x	15 m, 30 m		

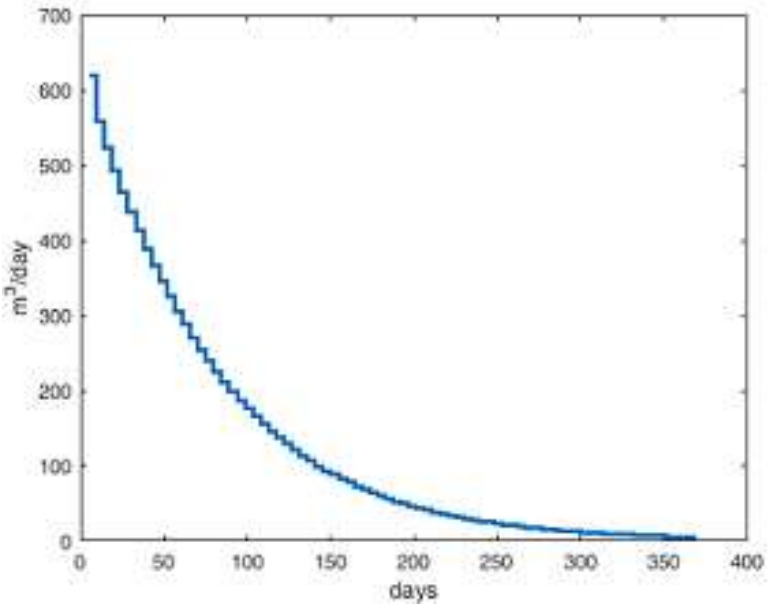

Figure 13. Fluid flow rate at zero ultrasound energy.

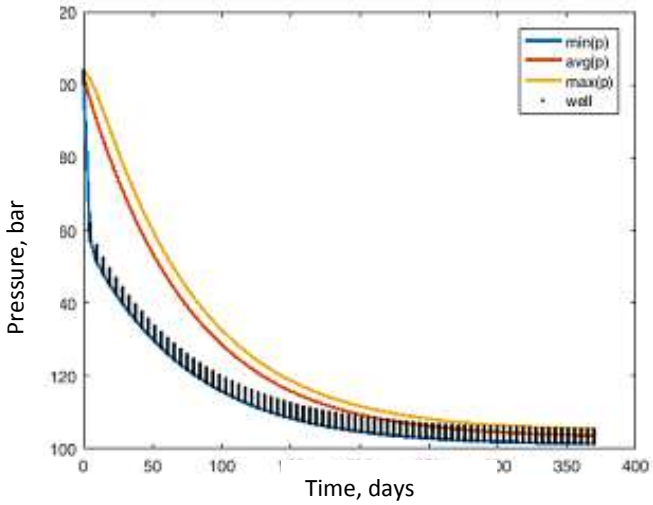

Figure 14. Reservoir pressure at zero ultrasound energy.

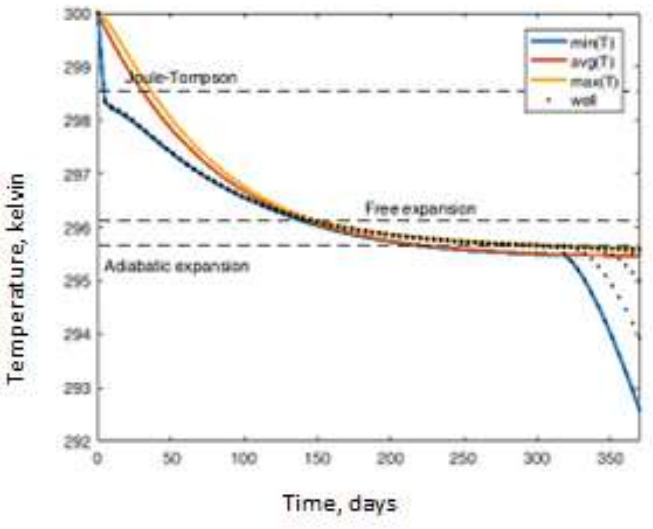

Figure 15. Reservoir temperature at zero ultrasound energy.

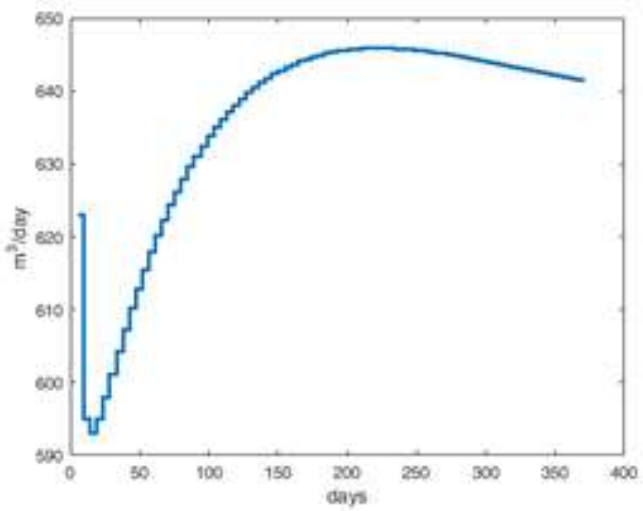

Figure 16. Flow rate at 15 m and 5 kW.

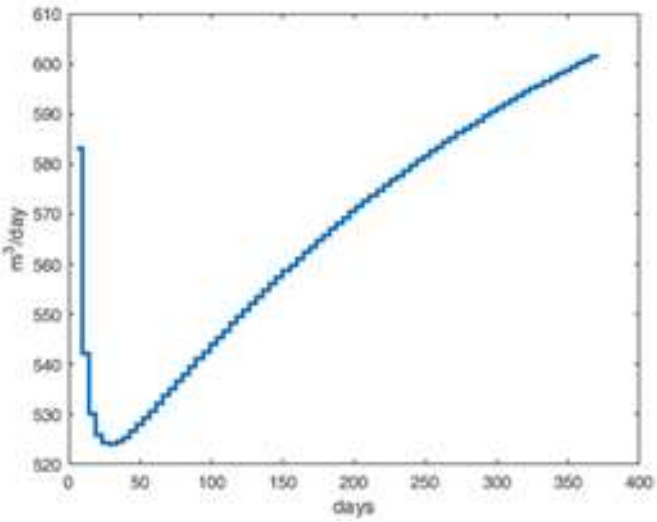

Figure 17. Flow rate at 30 m and 5 kW.

energy was applied. Continuous drop in reservoir temperature with time for the three expansion processes (Joule-Thomson, linearized adiabatic and free expansion) were observed when external energy was not applied to the reservoir as shown in Figure 15. After ultrasound energy was applied to the reservoir an improvement in reservoir fluid flow rate, pressure and temperature was observed and these consequently led to improve oil recovery. However, the following factors affect the efficiency of the ultrasound energy:

(i) Propagation distance (reservoir coverage)
(ii) Reservoir rock properties (porosity and permeability)
(iiii) Output power intensity

The above-mentioned factors that affect the efficiency of the ultrasound energy with regards to improving oil recovery can be addressed by increasing the ultrasound power intensity.

Propagation distance/Reservoir coverage

The reservoir fluid flow rate, pressure and temperature improved when ultrasound energy of 5 kW output power was introduced into the reservoir. The ultrasound waves propagation distance (reservoir coverage) was set at 15 m. Figures 16, 18, and 20 shows the reservoir fluid flow rate, pressure and temperature respectively at 5 kW

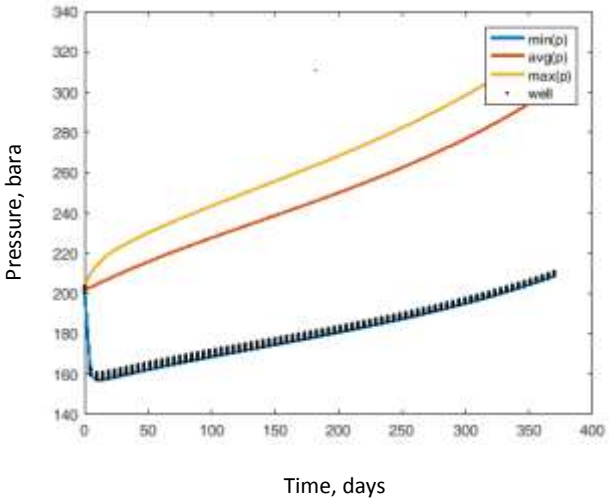

Figure 18. Reservoir pressure at 15 m and 5 kW.

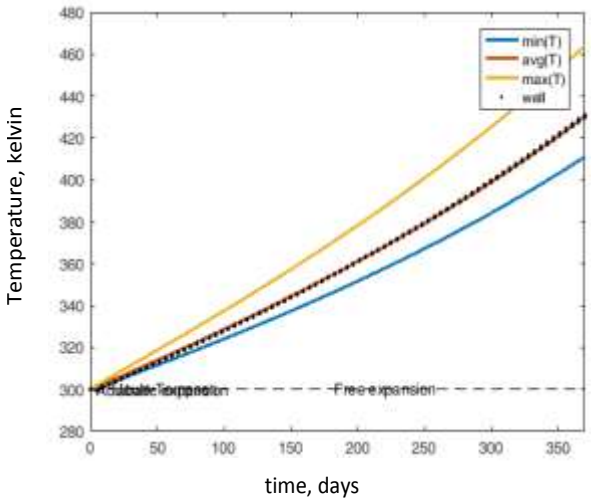

Figure 20. Reservoir temperature at 15 m and 5 kW.

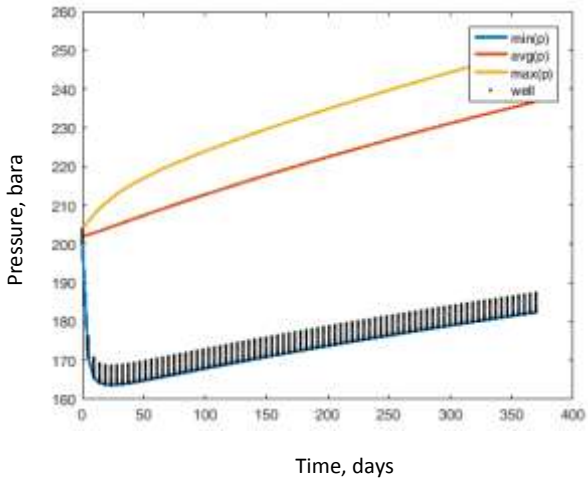

Figure 19. Reservoir pressure at 30 m and 5 kW.

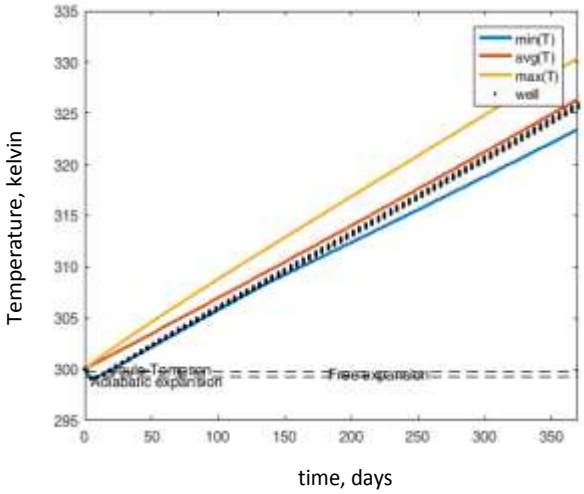

Figure 21. Reservoir temperature at 30 m and 5 kW.

ultrasound output power intensity and 15 m propagation distance. But when the propagation distance was increased to 30 m, the reservoir fluid flow rate, pressure and temperature reduced, (Figures 17, 19 and 21) respectively. This reduction is as a result of the attenuation of the ultrasound energy with distance. Example, the flow rate at 15 m propagation distance for the first hundred days is 640 m^3/day (Figure 16) while at 30 m distance the flow rate is 545 m^3/day as shown in Figure 17.

The results in Figures 18 and 19 show a decrease in reservoir pressure with time at a propagation distance of 15 and 30 m respectively. The average reservoir pressure at 15 m propagation distance for the first hundred days is 220 bara (Figure 18) while at 30 m distance the pressure is 207 bara as shown in Figure 19.

The plots in figures 20 and 21 show a decrease in reservoir temperature with time when the propagation distance was increased from 15 m to 30 m respectively. The results in Figures 20 and 21 show a decrease in reservoir temperature for all the three expansion temperatures (Joule-Thomson, linearized adiabatic and free expansion) with time when the propagation distance is increased from 15 to 30 m. At the 15 m distance the average temperature is 324 K while at the 30 m distance it is 306 K.

Reservoir rock properties (porosity and permeability)

The rate of absorption and propagation velocity of ultrasound waves in any medium increases with a

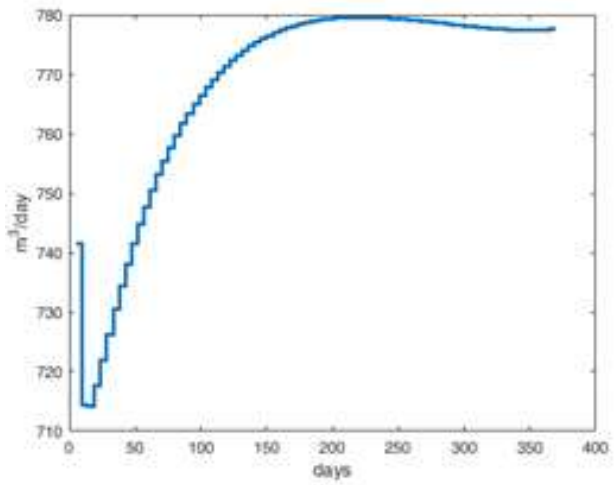

Figure 22. Flowrate at 15 m, 5 kW and 0.18- 0.30 porosity distribution.

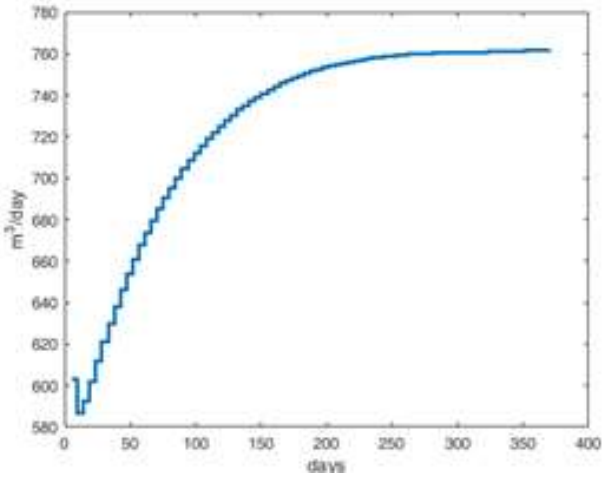

Figure 23. Flowrate at 15 m, 5 kW and 0.21-0.31porosity distribution.

decrease in the density of the medium; in other words, the rate of sound waves absorption in a medium is inversely proportional to the density of the medium. Obviously, increasing reservoir porosity and/or permeability will result in a decrease in reservoir rock bulk density. Results obtained from the simulation runs show that flowrates drop when the porosity distribution values were increased from 0.18-0.20 to 0.21-0.31 to 0.22-0.35 as shown in Figures 22, 23 and 24 respectively. The reservoir pressure also decreases with an increase in the values of porosity distributions, Figures 26, 27 and 28.

When ultrasound energy is absorbed by a medium, the sound energy is converted into heat energy. Results obtained from the simulation runs show a slight increase

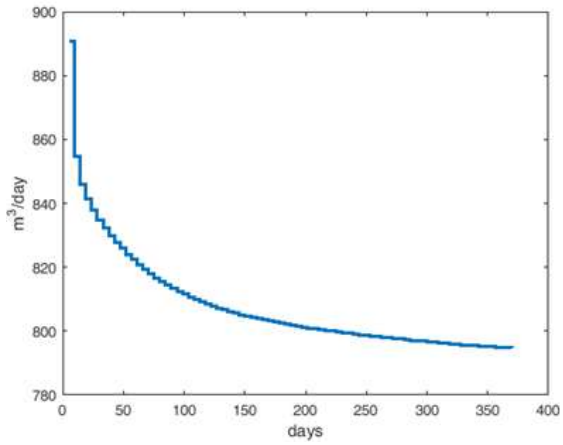

Figure 24. Flowrate at 15 m, 5 kW and 0.22- 0.35 porosity.

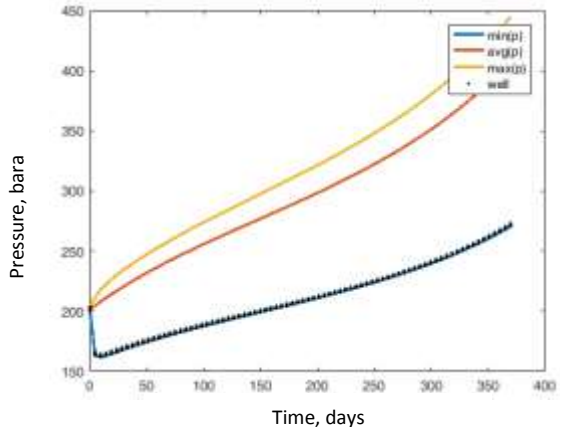

Figure 25. Reservoir pressure at 15 m, 5 kW and 0.18 - 0.30 porosity distribution.

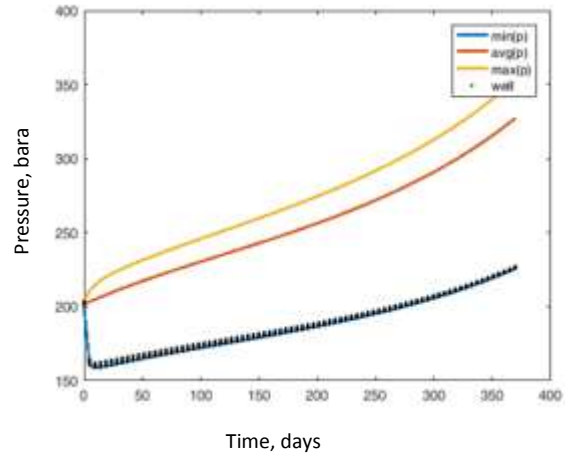

Figure 26. Reservoir pressure at 15 m and 0.21-0.31 porosity and 30-130 md permeability.

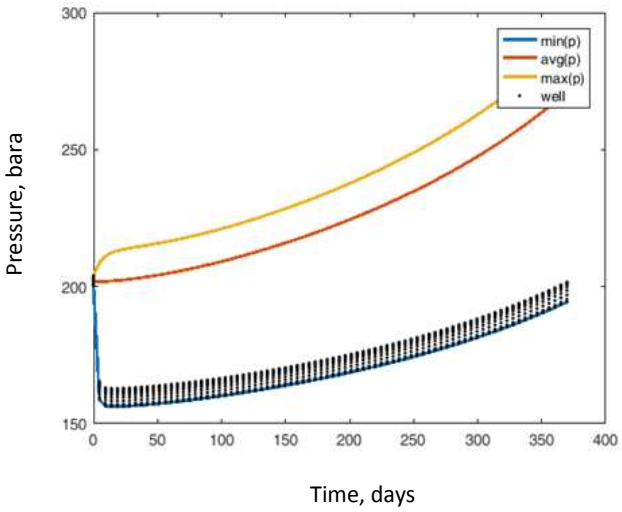

Figure 27. Reservoir pressure at 15 m and 0.22-0.35 porosity and 40- 220 md permeability.

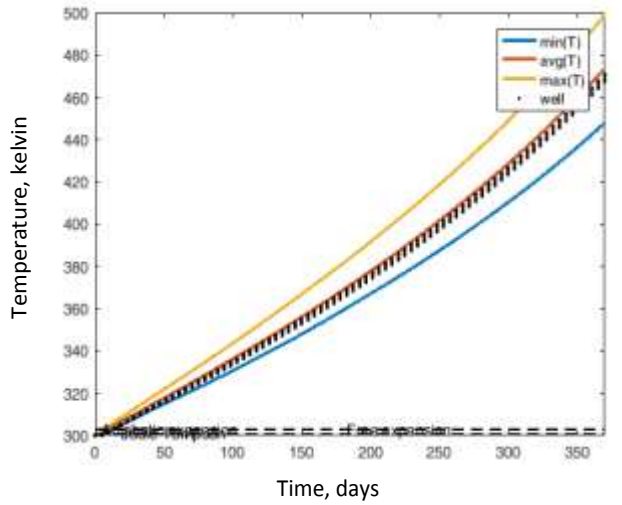

Figure 28. Reservoir temperature at 15 m and 0.18-0.30 porosity.

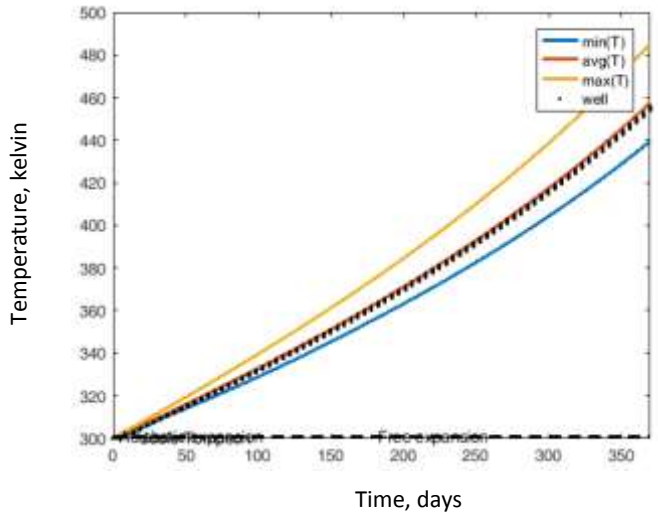

Figure 29. Reservoir temperature at 15 m and 0.21-0.31 porosity.

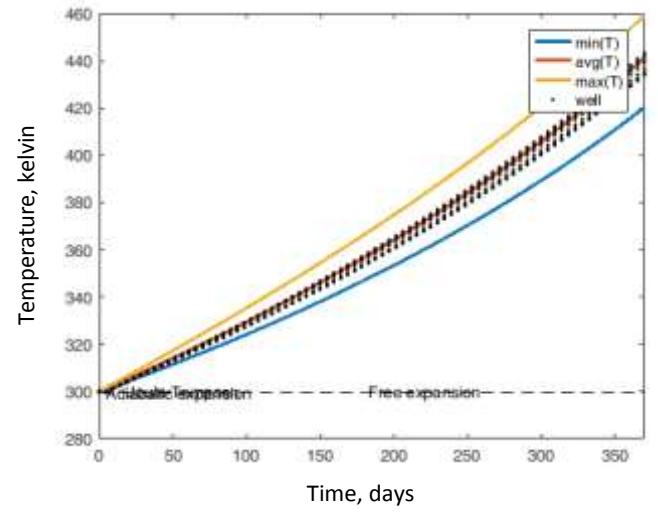

Figure 30. Reservoir temperature at 15 m and 0.22-0.35 porosity.

in reservoir temperature when porosity values were increased as depicted in Figures 29, 30 and 31. From Figures 29, 30 and 31 the temperature rise with time for the first hundred days are 325 K, 332 K and 333 K respectively.

Usually, permeability increases with porosity. However, some factors such as; tortuosity and specific surface area have little effect on the internal consistency of the porosity-permeability relationship. In this research work, the Carman-Kozeny equation was used to model permeability from porosity which shows a direct relationship. Therefore, the effect of permeability on ultrasound performance is nearly similar to that of porosity. Moreover, in this research work, homogeneous anisotropic permeability tensor (kx, ky and kz) was tested and similar a trend with the Carman-Kozeny permeability was observed.

Output power intensity

The intensity of an ultrasound beam at any point in a medium is the amount of energy exerted on the particles of the medium making them vibrate. The particles of the medium then possess energy by virtue of their oscillatory motion. The ultrasound power is the intensity per unit area. The plots in Figures 32, 33 and 34 show that

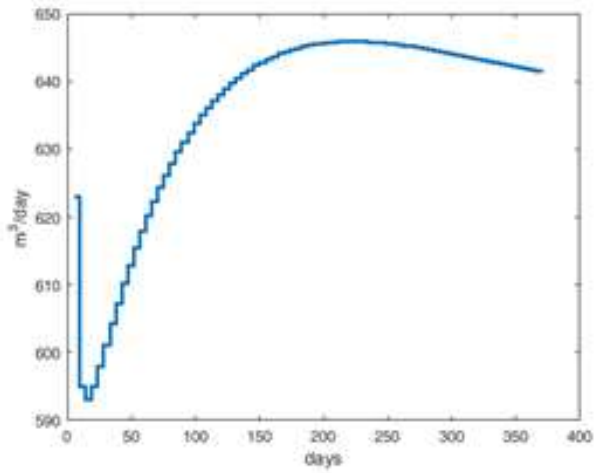

Figure 31. flow rate at 15 m and 5 kW.

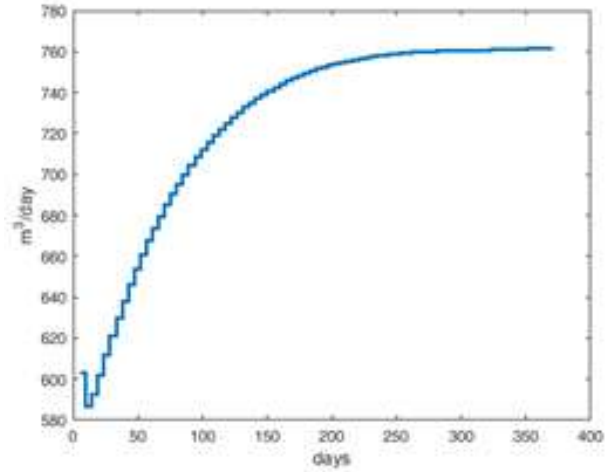

Figure 32. flow rate at 15 m and 6 kW.

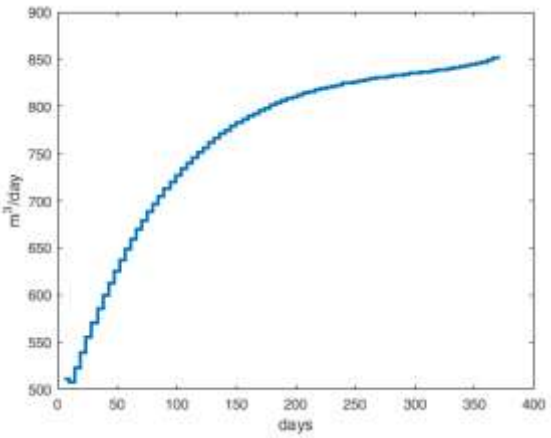

Figure 33. flow rate at 15 m and 7 kW.

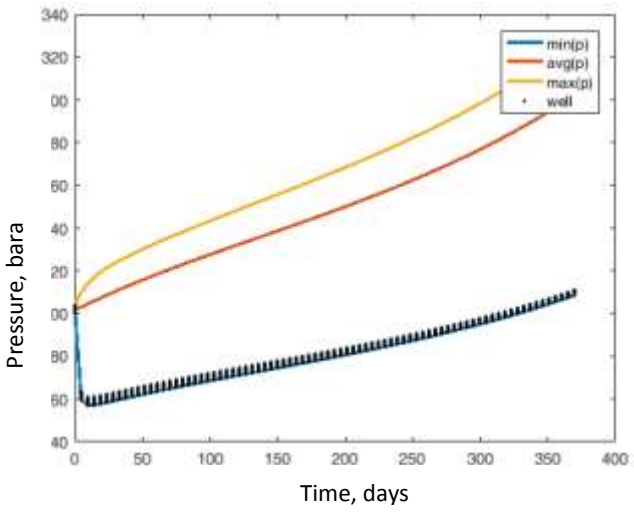

Figure 34. Pressure at 15 m and 5 kW.

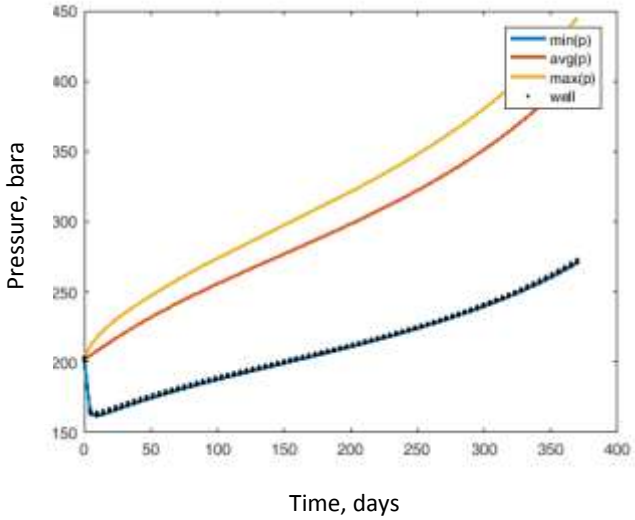

Figure 35. Pressure at 15 m and 6 kW.

increasing the ultrasound power intensity from 5 kW to 6 kW and to 7 kW caused an increase in the reservoir fluid flowrates. At the first hundred days of the ultrasound stimulation, flowrates of 630, 720 and 750 m^3/day were obtained for the 5, 6 and 7 kW respectively.

The average reservoir pressure at day hundred also increases from 220 250 bara and to 290 bara for the 5, 6 and 7 kW power as shown in Figures 35, 36 and 37 respectively.

The average reservoir temperature for the three expansion processes shows an increment with ultrasound power. From the plots in Figures 38, 39 and 40 the average temperature increases from 325 K at 5 kW to 335 K at 6 kW and then to 342 K at the 7 kW

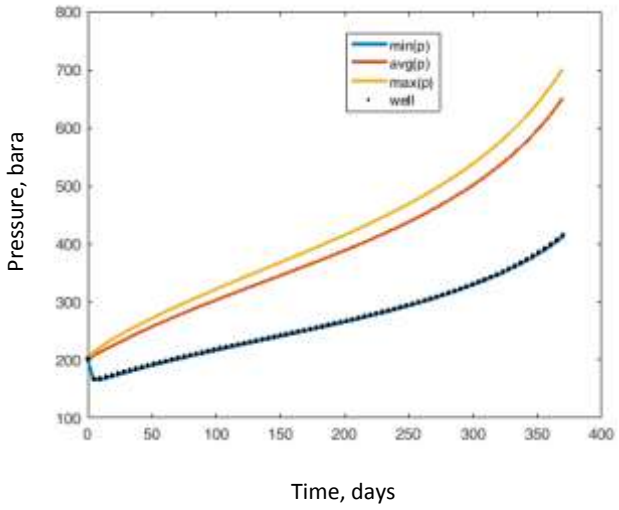

Figure 36. Pressure at 15 m and 7 kW.

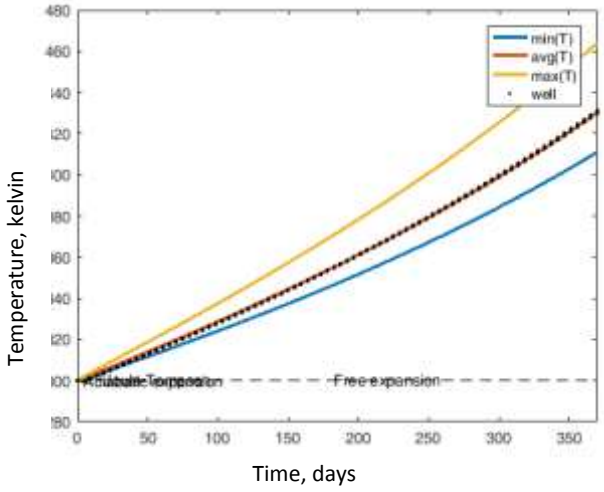

Figure 37. Temperature at 15 m and 5 Kw.

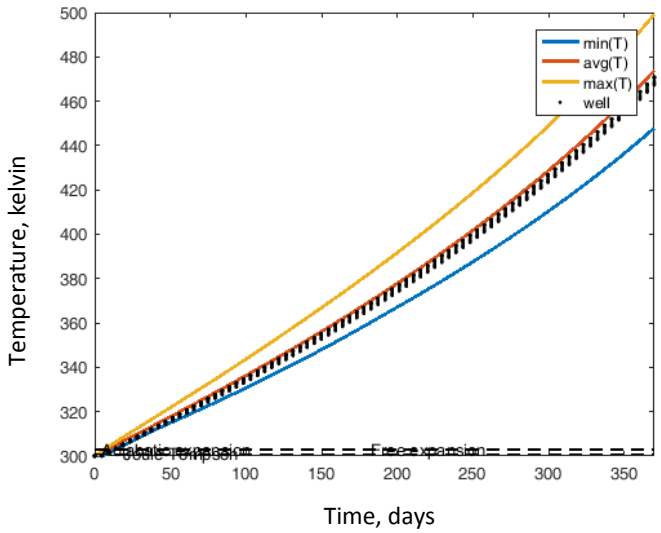

Figure 38. Temperature at 15 m and 6 kW.

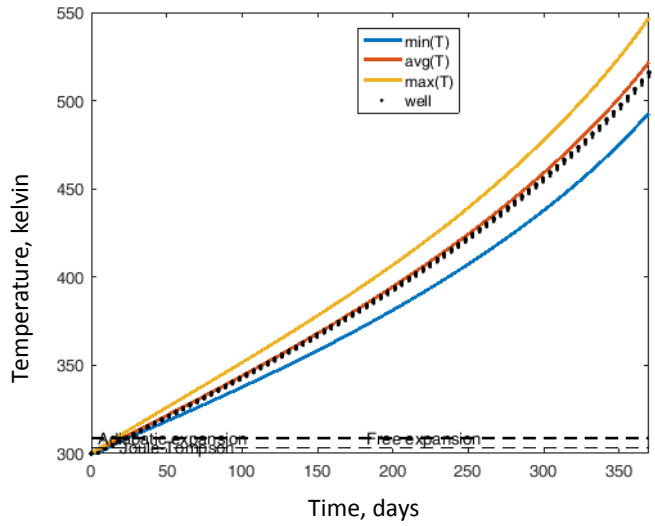

Figure 39. Temperature at 15 m and 7 kW.

power. The reservoir temperature also increases with time when the ultrasound power is increased. Figures 38, 39 and 40 show the results for the three expansion processes. Figure 41 shows the reservoir pressure distribution with the effect of ultrasound energy.

Effects of induced stress on the rock pore throat by ultrasound energy

The stress exerted on the pore walls of the reservoir rock by the ultrasound energy may have effects on the rock compressive strength. This can result in deformation of the pore throat or may even lead to grain slippage or fracture if excessive ultrasound power intensity is applied.

Figures 42 and 43 show the stress distribution and the corresponding strain distribution respectively.

Conclusion

Ultrasound waves energy can be used to simulate oil production from a reservoir. In other words, it can be applied as a means of improving oil recovery. Before carrying out ultrasonic oil recovery project, it is imperative to perform some preliminary studies. These studies include; software simulation, laboratory experiment and field pilot test. Software simulation should be the initial

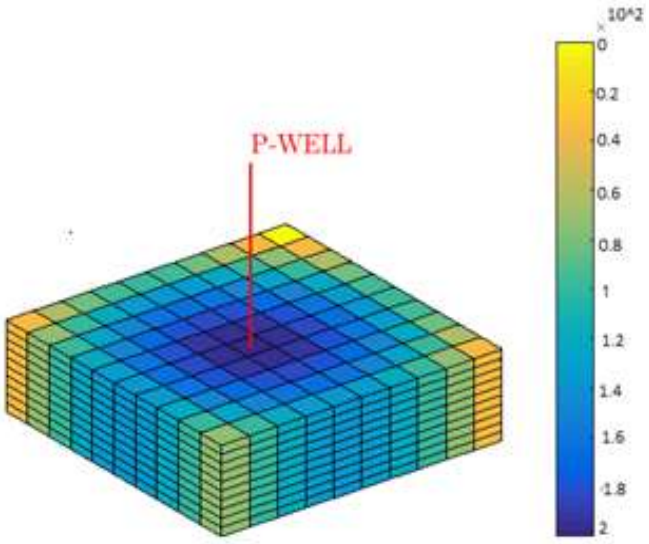

Figure 40. Effective pressure distribution in the reservoir.

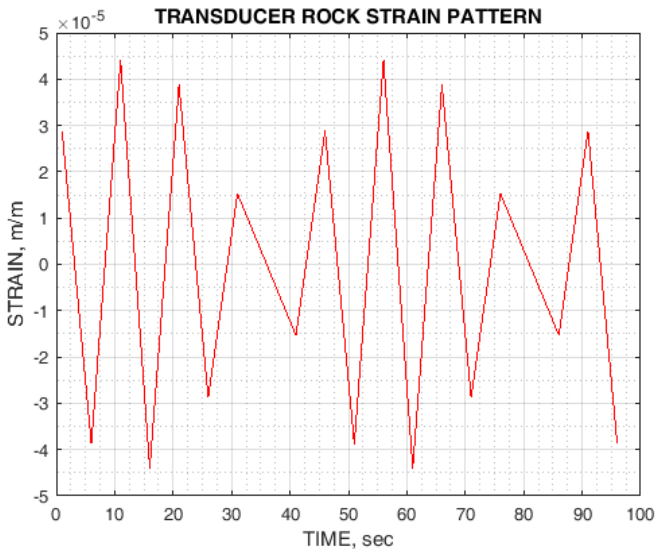

Figure 42. Ultrasound induced strain on the rock.

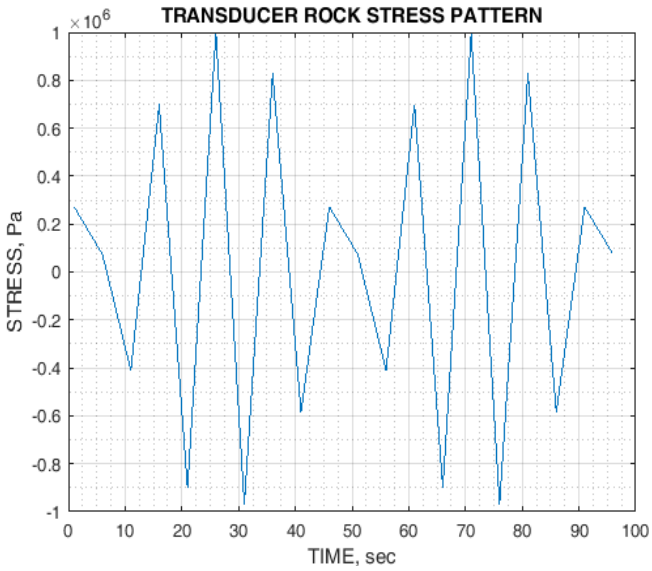

Figure 41. Ultrasound induced stress on the rock.

stage of the ultrasound project due to the fact that it is faster, cheaper, less risk and more flexible than laboratory experiment and pilot test and will also provide insight and a quick view of the ultrasound energy effect on any given reservoir. In this research work, MRST has been demonstrated to be an effective tool for simulating the application of ultrasound technology on improving oil recovery. The following were observed after simulation runs:

(i) Propagation distance affects the performance of the ultrasound waves. This effect can be compensated by increasing the ultrasound power intensity.
(ii) Higher porosity and permeability values also affect the performance of the ultrasound process. This effect is also compensated by increasing the ultrasound power intensity.
(iii) Ultrasound energy can increase reservoir rock compressive and tensile stress. Therefore, care has to be taken to avoid exerting excessive stress on the rock from applying high power intensity.

CONFLICT OF INTERESTS

The authors have not declared any conflict of interests.

REFERENCES

Aarts AC, Gijs O, Bot ET (1999). Enhancement of liquid flow through a porous media by ultrasonic. SPE. European Petroleum Conference, 20-22 October, The Hague, Netherlands.
Abramova A, Vladimir A, Vadim B, Artyom G, Pashin D (2014). Ultrasonic technology for enhanced oil recovery. Scientific Research in Engineering 6:177-184.
Alhomadhi E, Amro M, Almobark M (2014). Experimnetal Application of Ultrasound Waves to Improve Oil Recovery During Waterflooding. Elsevier 26(1):103-110.
Chen W, Holm S (2003). Modified Szabo's wave equation models for lossy media obeying frequency power law. The Journal of the Acoustical Society of America 114(5):2570-2574.
Christine D (2013). User's guide for hysteretic capillary pressure and relative permeability functions in TOUGH2. California: Earth service devision lawrence berkeley national laboratory. https://www.osti.gov/biblio/1164322
Delong X, Jinjing D, Chao L, Lixin B (2014). Research on viscosity reduction of oil in water for ultra heavy crude oil by using ultrsonic wave. 21st International congress on sound and vibration, Institute of Acoustics, Chinese Academy of Sciences, Beijin, China 100190, 13-17 July. http://english.ioa.cas.cn/rh/as/201408/W020140812320401902872.pdf

Dvorkin J (2009). Kozeny-Carman equation revisited. Retrieved from Geological Sciences/Stanford School of Earth, Energy and Environmental Sciences: https://pangea.stanford.edu. on 23/11/2018.

Erfan M, Mohammad AS, Ahmad KI (2011). Enhancing oil recovery through application of ultrasonic assisted waterflooding. Society of Petroleum Engineers (SPE 145014) Asia Pacific Oil and Gas Conference and Exhibition, Jakarta Indonesia, 20-22 September.

Knut-Andreas L (2016). An introduction to reservoir simulation using MATLAB - User Guide for the Matlab Reservoir Simulation Toolbox. Oslo, Norway: SINTEF ICT, Department of Applied Mathematics.

Mohammadian E, Junin R, Rahmani O, Idris AK (2013). Effects of Sonification radiation on oil recovery by ultrasonic waves stimulated waterflooding. Elsevier 53(2):607-614.

Mohammed M, Mahmoud M (2015). Extended model for ultrasonic-based enhanced oil recovery with experimental validation. Ultrasonic Sonochemistry, Elsevier 23:413-423.

Mullakaev MS, Abramov VO, Abramov AV (2015). Development of ultrasonic equipment and technology for well stimulation and enhanced oil recovery. Elsevier 125:201-208.

Naderi K, Babadagli T (2010). Influence of Intensity and Frequency of Ultrasonic Waves on Capillary Interaction and Oil Recovery from Different Rock Types. Elsevier 17(3):500-508.